Hybrid nanocrystalline TiO 2 solar cells with a fluorene–thiophene copolymer as a sensitizer and hole conductor

P. Ravirajan, S. A. Haque, J. R. Durrant, D. Poplavskyy, D. D. C. Bradley, and J. Nelson

Citation: Journal of Applied Physics **95**, 1473 (2004); doi: 10.1063/1.1638614
View online: http://dx.doi.org/10.1063/1.1638614
View Table of Contents: http://scitation.aip.org/content/aip/journal/jap/95/3?ver=pdfcov
Published by the AIP Publishing

Hybrid nanocrystalline TiO_2 solar cells with a fluorene–thiophene copolymer as a sensitizer and hole conductor

P. Ravirajan[a)]
Centre for Electronic Materials and Devices, Department of Physics, Imperial College London, Prince Consort Road, London SW7 2BW, United Kingdom and Department of Physics, University of Jaffna, Jaffna, Sri Lanka

S. A. Haque and J. R. Durrant
Centre for Electronic Materials and Devices, Department of Chemistry, Imperial College London, Exhibition Road, London SW7 2AZ, United Kingdom

D. Poplavskyy, D. D. C. Bradley, and J. Nelson
Centre for Electronic Materials and Devices, Department of Physics, Imperial College London, Prince Consort Road, London SW7 2BW, United Kingdom

(Received 29 July 2003; accepted 11 November 2003)

We report the effects of layer thickness, interface morphology, top contact, and polymer–metal combination on the performance of photovoltaic devices consisting of a fluorene–bithiophene copolymer and nanocrystalline TiO_2. Efficient photoinduced charge transfer is observed in this system, while charge recombination is relatively slow ($\sim$100 μs–10 ms). External quantum efficiencies of 13% and monochromatic power conversion efficiencies of 1.4% at a wavelength of 440 nm are achieved in the best device reported here. The device produced an open-circuit voltage of 0.92 V, short-circuit current density of about 400 $\mu A\,cm^{-2}$, and a fill factor of 0.44 under simulated air mass 1.5 illumination. We find that the short-circuit current density and the fill factor increase with decreasing polymer thickness. We propose that the performance of the indium tin oxide/TiO_2/polymer/metal devices is limited by the energy step at the polymer/metal interface and we investigate this situation using an alternative fluorene-based polymer and different top contact metals. © *2004 American Institute of Physics.* [DOI: 10.1063/1.1638614]

I. INTRODUCTION

Solar cells based on organic electronic materials are a subject of increasing interest. The possibility of manufacturing devices directly from solution offers the prospect of very low cost manufacture of plastic solar cells on flexible substrates. Additional advantages are small material requirements, low weight, choice of color and a wide range of applications.[1–7] Power conversion efficiencies exceeding 3% have now been achieved in several organic device configurations.[8–10] All of these are based on a heterojunction between an electron transporting (acceptor) and a hole transporting (donor) component, combined in either a planar structure or a blend. Factors which limit performance at present include poor photostability of the active layers, phase segregation, and low mobility of charge carriers, particularly electrons. One approach is to use *inorganic* semiconductor nanoparticles[11] or nanorods[1] as the electron transport component. Nanostructured metal oxides such as TiO_2 and ZnO are particularly interesting because of the ease of fabrication, good control of film morphology[2] and interfacial properties,[12] mechanical and chemical stability, and low cost. Simple procedures allow the fabrication of rigid, connected porous metal oxide films which can be sensitized with light absorbing dyes and/or filled with a hole-transporting material. This approach allows good electrical connectivity to be combined with large interfacial area, which is needed for effective charge separation, and has been exploited in dye sensitized devices.[7,9,13] More recently, sensitization of metal oxides by conjugated polymers has been studied for several materials combinations, including poly(2-methoxy-5-(2′-ethyl-hexyloxy) paraphenylene vinylene)(MEH–PPV)/TiO_2,[14–18] poly(*N*-phenylimino-1,4-phenylene-1,2-ethenylene-1,4-(2,5-dioctoxy)-phenylene-1,2-ethenylene-1,4-phenylene)(PA–PPV)/TiO_2,[19] MEH–PPV/SnO_2,[15,20] and polyalkylthiophene(PAT)/TiO_2.[21,22] In this approach, the conjugated polymer serves two purposes, absorption of light and transport of holes, thus removing the need for a separate light absorbing component, such as dye molecules.

Photovoltaic devices made from TiO_2/polymer combinations sandwiched between indium tin oxide (ITO) and Au electrodes have been reported by several groups.[16–19,22] Although reported peak quantum efficiencies reach 25%,[19] the air mass (AM) 1.5 power conversion efficiency is still low ($<$1%). In most cases these were planar structures where charge separation occurs only at the flat TiO_2/polymer interface, and performance was limited by poor hole mobility of the polymer and low interfacial area. Attempts to increase the interfacial area using dispersed nanocrystals[23,24] have been limited by poor electron transport between separate nanocrystals, and attempts to use nanocrystalline films[16,22,25] have been limited by poor polymer penetration into the porous film. An alternative approach using an *in situ* growth of

a)Electronic mail: pr2@imperial.ac.uk

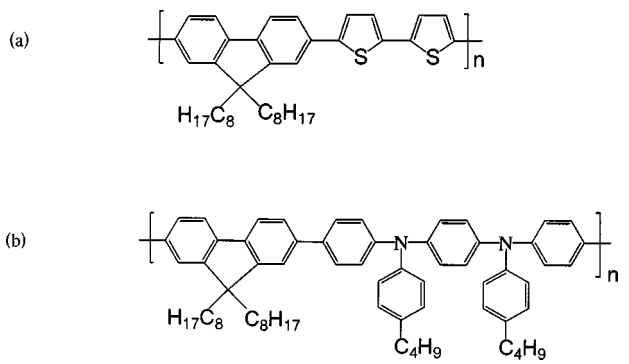

FIG. 1. Chemical structures of (a) poly(9,9-dioctylfluorene-co-bithiophene) (F8T2) and (b) poly (9,9-dioctylfluorene-*co*-bis-*N*,*N*′-(4-butyl phenyl)-bis-*N*,*N*′-phenyl-1,4-phenylenediamine) (PFB).

the TiO_2 network from an organic precursor[26] is promising but appears to be limited by poor electron transport in the amorphous TiO_2.

In this article, we study structures based on a high hole-mobility fluorene–bithiophene copolymer, poly(9.9-dioctylfluorene-co-bithiophene)(F8T2), and TiO_2 substrates of different morphology. We have recently reported that F8T2 polymer penetration into thick porous TiO_2 films can be controlled by melt processing and treatment of the TiO_2 surface.[27] Here, we show that penetration into thin porous films is achieved simply by dip coating, and we study the device characteristics as a function of device design. We show that (i) interface morphology, (ii) layer thickness, and (iii) matching of the polymer ionization potential to the electrode work function are all critical to device performance.

II. EXPERIMENT

A. Materials

Two hole-conducting polymers have been used in this work, poly(9,9-dioctylfluorene-co-bithiophene) (F8T2) and poly(9,9-dioctylfluorene-*co*-bis-*N*,*N*′-(4-butyl phenyl)-bis-*N*,*N*′-phenyl-1,4-phenylenediamine) (PFB). These materials were synthesized by the Dow Chemical Company and carefully purified to remove catalyst residues and other inorganic contaminants. F8T2 has a broad optical absorption in the visible spectrum peaking at about 470 nm, high hole-mobility,[28] and possesses a liquid crystal phase above 265 °C.[29] The other polymer, PFB, absorbs less strongly in the visible[30] and has a lower ionization potential I_P [5.1 eV (Ref. 31) compared to 5.5 eV for F8T2 (Ref. 32)]. The chemical structures of both polymers are shown in Fig. 1. Nanocrystalline TiO_2 films (15 nm diameter TiO_2 particles, 50% porosity) were prepared by spin coating a diluted aqueous TiO_2 colloidal paste. The colloidal paste was prepared as described in Ref. 33, using chemicals purchased from the Sigma-Aldrich Company.

B. Sample fabrication

All samples were prepared on ITO-coated glass substrates ($\sim$1 cm^2), which were first cleaned by ultrasonic agitation in acetone and isopropanol. The cleaned substrate was then covered with a dense TiO_2 layer, about 50 nm thick using spray pyrolysis.[34] This dense layer prevents direct contact between the polymer and the substrate, and is referred to as a ''hole-blocking layer (HBL).'' In some cases, a thin porous layer of nanocrystalline TiO_2 of thickness about 100 nm was deposited by spin coating a diluted aqueous colloidal paste onto the HBL. The layers were then sintered at 450 °C for 30 min in air. The polymer was applied by spin coating a solution (10–15 mg/ml) of polymer in toluene at 2000–4000 rpm resulting in polymer thicknesses of about 50–100 nm. The porous layer substrates were dip coated by immersing in a solution of F8T2 in toluene (2 mg/ml) at 50 °C for several hours prior to spin coating the polymer. The thickness of all the films was measured by a Tencor Alpha-Step 200 profilometer. For electrical characterization, gold, platinum, or aluminum electrodes were deposited onto the polymer film by thermal evaporation though a shadow mask. There were six devices per substrate to check reproducibility and the active area of each device was about 0.045 cm^2. For optical measurements, uncontacted samples on ITO substrates were used. Samples composed of the HBL and a polymer layer will be referred to below as bilayer samples, while those containing an extra porous TiO_2 layer with both dip- and spin coated polymer layers will be referred to as multilayer samples.

C. Optical measurements

Photoinduced charge transfer yield and recombination kinetics were measured for the TiO_2/F8T2 system using nanosecond–millisecond pump–probe transient optical spectroscopy, as described in Ref. 35. A nitrogen laser pumped dye laser was used as the excitation source (repetition rate 4 Hz, pulse duration $<$1 ns) and a tungsten lamp with a stabilized power supply as the probe light. The probe wavelength was selected with monochromators both before and after the sample. This minimized the amount of probe light incident on the sample and the amount of scattered light/photoluminescence emission reaching the photodetector. A high gain photodiode equipped with appropriate low- and high-pass filtering was employed as the detection unit and was coupled to a GOULD 475 digital storage oscilloscope and a computer for signal analysis. The pump wavelength was chosen to be 500 nm, close to maximum absorption of F8T2 polymer, and the probe wavelength 720 nm. The transient optical spectrum, which peaks at 725 nm, is assigned to the positive polaron in F8T2 after comparison with the absorption spectrum of chemically oxidized polymer samples, as shown in Fig. 2. We have performed detailed transient absorption studies on pristine F8T2 films as control experiments (excitation at 500 nm and probe at 720 nm). These studies reveal no evidence of any absorption feature, which could be assigned to the triplet, for instance, on a time scale of charge recombination dynamics (0.1 μs–100 ms). Therefore, the decay in absorbance as a function of time after the excitation is attributed to recombination of F8T2 polarons with electrons to the TiO_2 by photoinduced charge transfer.

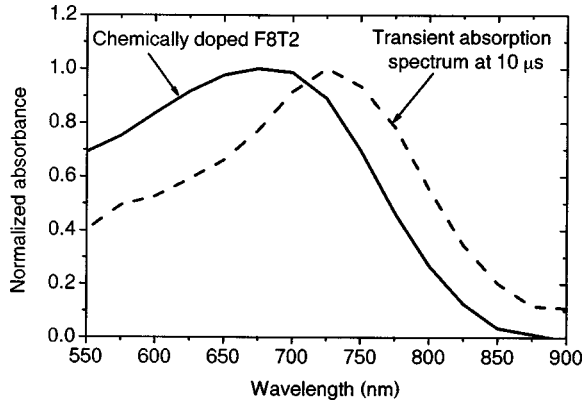

FIG. 2. F8T2 cation absorption spectra recorded following chemical oxidation with $FeCl_3$ (solid line) and following photoinduced charge separation (dashed line). The former was measured in solution (toluene) and in the presence of $FeCl_4^-$ counterions.

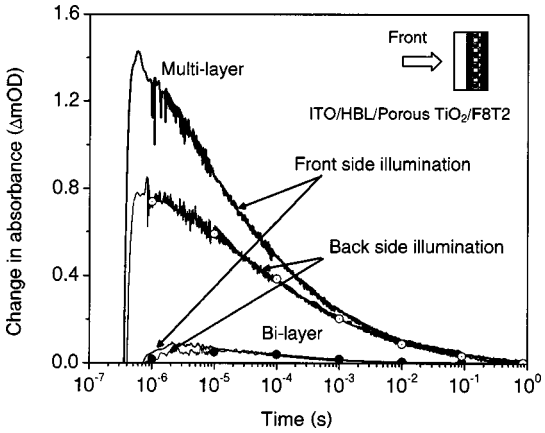

FIG. 3. Transient absorption kinetics following the positive polaron state absorption of F8T2 on top of a TiO_2 nanocrystalline layer. Inset shows the sample structure ITO/HBL/porous TiO_2 /F8T2^d/F8T2^s where superscript "d" indicates dip coated and "s" is spin coated. The excitation density was about 30 μJ/pulse/cm^2 (corresponding to 1.3×10^{14} incident photons/pulse/cm^2) and the decay is assigned to recombination between electrons donated to the TiO_2 following photogeneration and positive polarons in F8T2. Solid lines indicate front surface illumination and solid lines with symbols correspond to back-surface illumination.

D. Electrical measurements

Photovoltaic performance of the devices was studied by measuring photocurrent spectra and current density–voltage ($J-V$) characteristics under light illumination. For electrical characterization, the devices were housed in a home built sample holder with a quartz window. The sample holder was evacuable to a pressure of $<10^{-1}$ mbar and all the measurements were taken under vacuum. The light source was a 100 W xenon lamp, which was driven by a Bentham 505 stabilized power supply. The light from the lamp was dispersed by a CM110, 1/8 m monochromator, which was controlled by computer. Current and voltage measurements were taken using a computer controlled Keithley 237 high voltage source measure unit (SMU). External quantum efficiency spectra were calculated from short-circuit photocurrent spectra by comparison of the photoresponse with that of a calibrated silicon photodiode (Newport). Monochromatic $J-V$ measurements were taken at the wavelength that gave the highest photocurrent. Reverse and forward bias measurements were carried out separately with a voltage step size of 0.02 V. Forward bias corresponds here to ITO biased negatively with respect to the counterelectrode. $J-V$ characteristics in the dark were measured both before and after the measurements of the illuminated $J-V$ characteristics in order to confirm that the device behavior was not changed by illumination. $J-V$ characteristics were also taken under simulated sunlight using a home built computer controlled potentiostat measurement unit and a halogen lamp calibrated to AM 1.5 equivalent intensity (100 mW cm^{-2}).

E. Electroabsorption measurements

The electroabsorption technique was used to find the built-in voltage, V_{BI}, of the single polymer layer devices. In this technique, the absorption of the device is modulated by an externally applied ac voltage, V_{ac} and the relative change in its transmittance, $\Delta T/T$, which is proportional to the change in absorption, and is measured as a function of the wavelength λ of the incident light and dc bias voltage V_{dc}. The electroabsorption signal at the resonance wavelength at the frequency of modulating ac voltage is proportional to the product $V_{ac}\times(V_{dc}-V_{BI})$. This allows us to determine the built-in voltage by measuring $\Delta T/T$ as a function of V_{dc} at a fixed value of V_{ac} (see, e.g., Ref. 36). A xenon lamp with a CM110 monochromator was used as the light source. The light was incident on the device through the ITO side, reflected back from the top contact of the device, and detected by a Si photodiode. The modulation frequency was 5 kHz, and V_{ac} was varied in the range 0.2–1 V. The dc response from the photodetector, the transmittance T, was measured by a BlackStar 4503 digital voltmeter while the modulated change in transmittance ΔT was measured by an EG&G 5210 lock-in amplifier, equipped with a high gain I/V preamplifier (EG&G model 5182).

III. RESULTS AND DISCUSSION

A. Charge separation

Transient absorption kinetics for bilayer and multilayer samples on ITO coated glass are shown in Fig. 3. For both samples the HBL thickness is 50 nm and the effective polymer thickness is 50 nm. The effective polymer layer thickness on dense TiO_2 was estimated from the UV–VIS optical absorption of the layer and the known absorption coefficient of the polymer, measured on spectrosil. The interfacial area of the multilayer device was increased relative to the bilayer device on account of the ~100-nm-thick porous TiO_2 layer. The strong transient optical signal indicates high charge separation efficiency, estimated, from polaron absorbance, to be of order unity for the multilayer sample. The stronger signal for the multilayer compared to the bilayer sample is entirely consistent with higher charge separation efficiency, due to the larger interfacial area of the multilayer sample. Comparison of signals for illumination from the back (polymer side) and front (TiO_2 side) allows us to estimate the extent of polymer penetration into the film, since poor polymer penetration would leave a layer of polymer on the back-

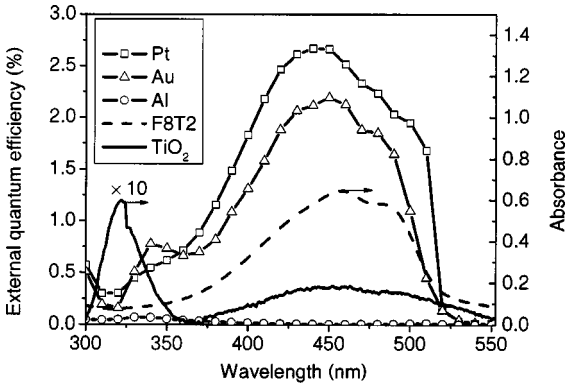

FIG. 4. Quantum efficiency spectra of TiO_2/F8T2 bilayer devices with different top contacts. Absorbance spectra of F8T2 polymer film of thickness 50 nm on ITO (dashed line) and dense TiO_2 of thickness 50 nm on ITO (solid line) are also shown for comparison. The absorption spectrum of TiO_2 has been scaled by a factor of 10 so that it can be more readily seen.

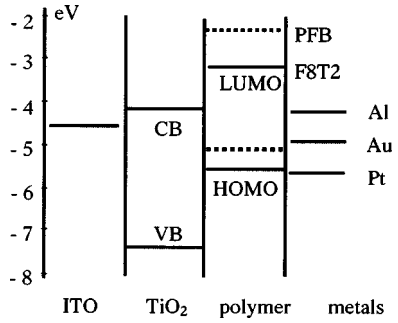

FIG. 5. Proposed electronic energy-level diagram for ITO/TiO_2/polymer/metal solar cell. HOMO and LUMO levels of F8T2 and PFB are shown by solid lines and dotted lines, respectively.

side of the film and lead to a lower charge separation yield due to the filtering of pulse light by that layer. Similar signals for back- and frontside illumination for the multilayer sample in Fig. 3, therefore, indicate effective penetration of the polymer into the porous TiO_2. The decay of the signal is relatively slow, with a half time of $\sim 100\ \mu s$, indicating slow polaron–electron recombination. This figure compares well with values reported for polymer–fullerene blends (1–100 μs),[37] and dye sensitised solar cells (100 μs–1 ms).[35,38,39] For the thin porous TiO_2 films used in this work, additional melt-processing or surface modification steps were evidently not needed to achieve penetration of the polymer into the pores, unlike the case of thick porous films.[27]

B. Effect of top electrode

Figure 4 shows a comparison of external quantum efficiency (EQE) spectra for ITO/HBL/F8T2/metal bilayer devices with 50 nm HBL, 50 nm polymer, and different top electrodes. Comparison with the optical absorption spectra of the dense TiO_2 layer (solid line) and polymer layer (dashed line) on their own shows that the photocurrent is predominantly due to absorption in the polymer for the case of high-work-function electrode (Au or Pt) devices and due to absorption in TiO_2 in the case of the Al electrode. The peak quantum efficiencies at wavelengths near the absorption maximum of the polymer (470 nm) for devices with both Au and Pt contacts are about two orders of magnitude greater than for the Al contacted device. We note that the direction of the short-circuit current flow in the Al contacted device is opposite to that in the Au and Pt devices: electrons travel to the ITO in the Pt and Au devices, while holes travel to the ITO in the Al device.

This result can be understood by considering the appearance of the built-in voltage inside the polymer film due to the difference in work functions Φ between the ITO and the top metal electrode. The work function of the ITO substrates was found to be about 4.5 eV, as measured by the Kelvin probe technique. The question of the work function of top metal electrodes requires a more careful approach. While the work-function values for the metals can be found in the literature (see, e.g., Ref. 40), those values are measured on carefully cleaned (or atomically flat) surfaces in high vacuum. It is clear that the interface between a polymer and an evaporated metal film is far from ideal, as chemical reactions[41] or formation of a damage layer[42] can occur. It has been shown that, for example, the work function of Au on top of conjugated polymers may be smaller than the expected value of 5.1 eV by as much as 0.2–0.3 eV (see, e.g., Refs. 43 and 44). For this reason, we have performed electroabsorption studies on single-layer polymer-only devices with the aim of determining the work functions of evaporated Al, Au, and Pt electrodes at the contact with F8T2. The bottom electrodes were either ITO ($\Phi \sim 4.5$ eV) or ITO/PEDOT:PSS [$\Phi \sim 5.2$ eV (Ref. 45)]. Electroabsorption spectra of devices with Al top contacts exhibited a single strong peak at a wavelength of 514 nm, which scaled linearly with the dc bias voltage. This implied that the sample was free of traps and the signal was due to the bulk of the polymer film. The built-in voltage could be reliably measured yielding a value of about 4.4 eV for the work function of the Al electrode, close to the value for clean Al of 4.3 eV.[40] On the other hand, devices with Au and Pt electrodes exhibited additional peaks, the number and shape of which varied from sample to sample. Moreover, the amplitudes of these peaks did not always scale linearly with the dc bias voltage. In this case a reliable measurement of the built-in voltage, and correspondingly the work function of the top electrode, is not possible as there is apparently a strong contribution to the measured signal from interfacial regions in addition to that from the bulk. The origin of this additional interfacial contribution to the signal is not clear but could be due to several reasons such as morphological changes in the polymer during the evaporation process, or chemical reaction between the polymer and the metal due to a strong affinity between noble metals and sulfur, present in the polymer. Therefore, we tentatively assumed that the work function of Au on F8T2 was $\Phi_{Au} \sim 4.9$ eV, similar to other polymer systems,[43,44] while the work function of Pt on F8T2 was higher by 0.4 eV [according to the differences in literature values of Φ_{Pt} and Φ_{Au} (Ref. 40)], i.e., $\Phi_{Pt} \sim 5.3$ eV (Fig. 5). Based on the proposed work functions for the metals, there is a positive built-in voltage, $V_{BI} = \Phi_{metal} - \Phi_{ITO}$, inside the polymer film in Au and Pt devices, and a negative built-in voltage in devices with Al top contact.

Under illumination at short circuit, excitons generated in the polymer layer near the TiO_2/polymer interface transfer negative charge to the TiO_2 and positive polarons form within the polymer. The electrons flow through the TiO_2 to the ITO electrode and positive polarons through the polymer to the Au or Pt electrode, assisted by the built-in voltage. In the case of the Al electrode, the sign of the short-circuit current (i.e., the polarity of the device) was reversed, as would be expected from the opposite sign of V_{BI}. In this case positive charges will be attracted to the ITO and electrons to the Al contact, reversing the direction of the current. While the shape of the EQE spectrum of the Au device resembles the absorption spectra of both polymer and TiO_2, the EQE of the Al device resembles only the TiO_2 absorption spectrum. This suggests that the electron transport in the polymer is better than hole transport in the TiO_2. (The hole mobility in the porous TiO_2 was too low to be measured[46]). TiO_2 is known to trap holes at surface states, and this will be an important effect in nanocrystalline TiO_2. A second factor is the relatively high background doping of the weakly *n*-type TiO_2 (Ref. 46) compared to the intrinsic polymer, which will tend to reduce the magnitude of the built-in electric field in the TiO_2 layer. Therefore, the built-in voltage in the Al device helps the photogenerated electrons in TiO_2 travel through the polymer to the Al electrode, while photogenerated holes in F8T2 do not reach the ITO electrode through TiO_2 due to the very poor hole-transport in the TiO_2. Therefore, the EQE of the Al device only resembles the absorption of the TiO_2. On the other hand, in the Au contacted device, the built-in voltage, hole mobility of polymer, and electron mobility of TiO_2, all favor hole transport through polymer and electron transport through TiO_2, with the result that the EQE spectrum resembles the absorption spectrum of both materials. The very low quantum efficiency observed for the Al contacted device implies poor hole transport in TiO_2 and/or poor electron transport in F8T2.

These results support the fact that good hole-transmitting contacts between the polymer and the top electrodes are essential for efficient charge collection. Note that because TiO_2 is deposited on top of ITO in these structures, the polarity is reversed compared to most other organic photovoltaic devices, where holes flow towards the ITO. For efficient charge collection in our devices, high-work-function materials must be used for the hole collecting contact. The performance limitations caused by the energy step at the F8T2/Au contact are discussed in Sec. III D below.

C. Influence of interface morphology

Figure 6 compares external quantum efficiency spectra for bilayer and multilayer devices with different top contacts. For all samples the HBL thickness was about 50 nm and the effective polymer thickness 50 nm, while the multilayer devices contained an additional 100 nm porous TiO_2 layer, which was dip coated before spin coating. The multilayer Pt contacted device shows a peak quantum efficiency of about 11% at 440 nm and about 14% at 370 nm, while the Au contacted device shows a peak quantum efficiency of about 13% at 440 nm and about 15% at 340 nm. (The response below 387 nm, which is due to TiO_2, is not useful for solar illumination.) The highest quantum efficiency of the bilayer devices was only 2.7%. The improved quantum efficiency in the multilayer devices may be attributed to increased interfacial area due to the presence of the porous TiO_2 layer, as also supported by the transient optical measurements discussed above. High resolution scanning electron microscopy (SEM) images of dense and porous layers[46,47] clearly show that surface roughness is increased by adding the porous TiO_2 layer. This effect enhances the area available for exciton dissociation. The best monochromatic power conversion efficiency of a multilayer device with an Au electrode is 1.4% at 470 nm with a light intensity of 4.7 $mW\,cm^{-2}$. The device yielded an open-circuit voltage V_{OC} of 0.92 V, short-circuit current density J_{SC} of 400 $\mu A\,cm^{-2}$, and a fill factor of 0.44 under simulated sunlight of intensity 100 $mW\,cm^{-2}$ (see Fig. 7). However, the device photocurrent starts to fall off before the open-circuit voltage is reached. This ''kink'' in the $J-V$ characteristics was also observed in our bilayer devices with Au as a top contact, and has been seen before in other TiO_2/polymer/Au systems [ITO/TiO_2/MEH-PPV/Au,[16,18] ITO/TiO_2/PA-PPV/Au,[19] and ITO/TiO_2/BFB/Au (Ref. 48)], where the polymer has ionization potential of at least 5.3 eV, producing a significant energy step ($\geqslant$0.4 eV) at the polymer/Au interface. The kink in $J-V$ characteristics has

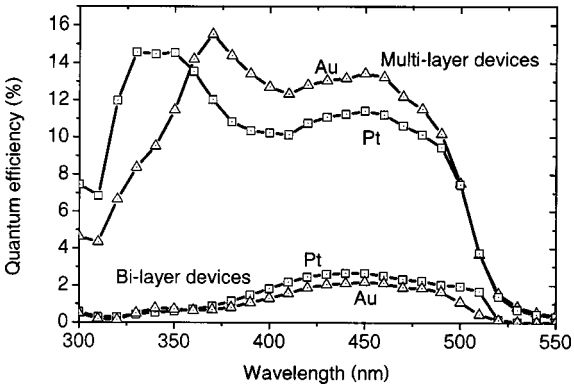

FIG. 6. Quantum efficiency spectra of TiO_2/F8T2 devices with different layer structures and top contacts, Au (triangles) and Pt (squares).

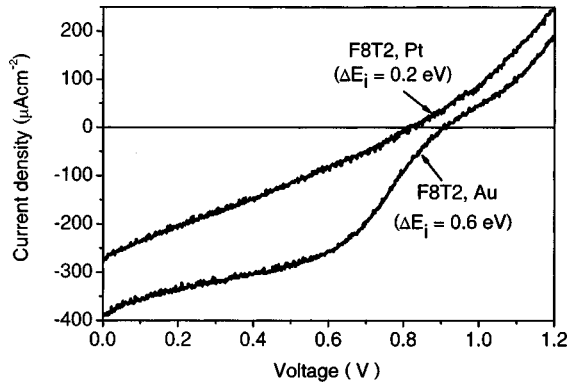

FIG. 7. $J-V$ characteristics of ITO/HBL(50 nm)/porous TiO_2 (100 nm)/F8T2^d/F8T2^s (50 nm)/metal solar cells under illumination by a solar simulator (100 $mW\,cm^{-2}$, air mass 1.5). Data are shown for Pt and Au metal electrodes. ΔE_i refers to the estimated energy step at the polymer–metal interface.

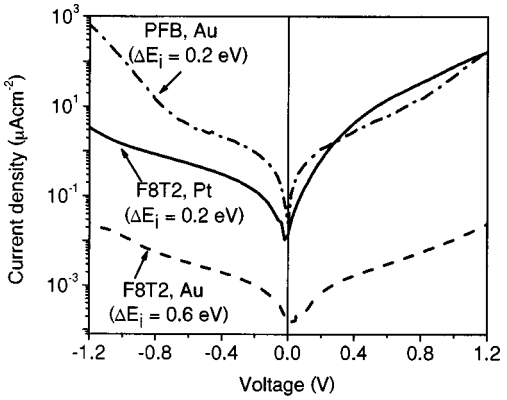

FIG. 8. $J-V$ characteristics of ITO/TiO_2/polymer/metal devices in the dark. Data are shown for PFB/Au, F8T2/Pt and F8T2/Au polymer/metal combinations.

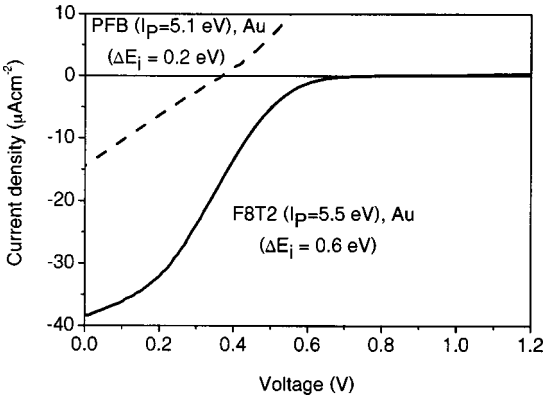

FIG. 9. $J-V$ characteristics of ITO/TiO_2/polymer/Au devices under monochromatic illumination at wavelengths corresponding to the maximum short circuit currents of the corresponding devices.

also been observed in molecular thin film solar cells (e.g., ITO/CuPc/C60/Al), where there is an energy step to hole injection from ITO to CuPc but disappears when PEDOT ($\Phi_{work}=5.3$ eV) is inserted between ITO and CuPc.[8] We have studied this effect under monochromatic illumination using different wavelengths with the same photocurrent generation rate (data not shown), and as a function of light intensity. The feature persists under different wavelengths, indicating that the kink is not a result of the spatial distribution of photogeneration. Moreover, the feature grows rather than diminishes with increasing light intensity, indicating that it is not due to charge trapping. However, the kink is not visible when the Au electrode is replaced with Pt, indicating that the kink is not due to the bulk properties of the polymer or the photogeneration profile but due to physical properties of the polymer/metal interface. Thus, the kink in $J-V$ characteristics of the Au device may be due to the energy step, ($\Delta E_i = I_P - \Phi$) at the F8T2 ($I_P=5.5$ eV)/Au ($\Phi=4.9$ eV) interface. We have further investigated this behavior using another fluorene-based polymer, PFB, as discussed below.

D. Effect of the energy step at the polymer/metal interface

In order to examine the effect of the interfacial energy step, ΔE_i, on the $J-V$ characteristics of the solar cell, we first reduced the energy barrier at the polymer/metal interface by replacing F8T2 polymer with PFB polymer, which has an ionization potential of 5.1 eV close to the work function of gold. Figure 8 compares dark $J-V$ characteristics of ITO/TiO_2/F8T2/Pt, ITO/TiO_2/F8T2/Au, and ITO/TiO_2/PFB/Au bilayer devices. All these devices had about 50 nm HBL and a similar polymer thickness. The very small dark current values in the ITO/TiO_2/F8T2/Au device compared to the other two devices can be attributed to a larger energy barrier for hole injection at the polymer/metal interface, illustrated by the energy level diagrams in Fig. 5. Since the open-circuit voltage of a solar cell is limited by, among other factors, currents injected from the electrodes opposing the photocurrent, we would expect a higher open-circuit voltage in the ITO/TiO_2/F8T2/Au device compared to the other two devices.

Figure 9 compares the $J-V$ characteristics of ITO/TiO_2/F8T2/Au and ITO/TiO_2/PFB/Au bilayer devices under monochromatic illumination at wavelengths corresponding to the maximum short-circuit currents of the corresponding devices. The absence of a kink in the $J-V$ curve for the PFB device further confirms that the kink in the $J-V$ curve of the ITO/TiO_2/F8T2/Au device is related to the significant energy barrier at the F8T2/Au interface. The origin of the kink in the $J-V$ curve is discussed in Ref. 49.

E. Effect of polymer thickness

Figure 10 shows the $J-V$ characteristics of ITO/HBL (50 nm)/porous TiO_2 layer (120 nm)/F8T2/Au devices with varying effective polymer thicknesses from 50 to 105 nm under simulated solar illumination of $\sim$100 mW cm^{-2} intensity. We estimated the effective polymer thickness on porous TiO_2 by comparing the optical absorption of the polymer coated TiO_2 electrode with the known absorption coefficient of the polymer on spectrosil, assuming the TiO_2 is $\sim$50% porous. Short-circuit current densities J_{SC} are highly dependent on the polymer thickness, increasing from 185 to 310 μA cm^{-2} when the polymer thickness is decreased from 105 to 50 nm, while V_{OC} remains approximately the same at a

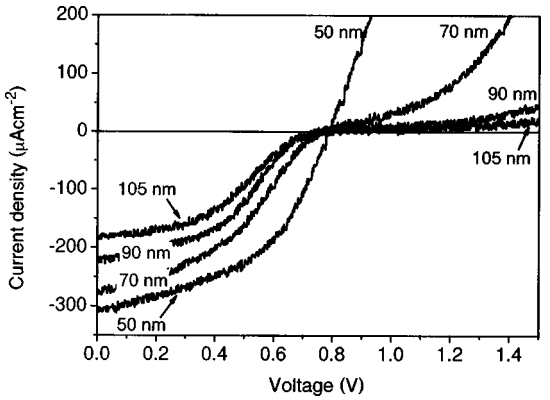

FIG. 10. $J-V$ characteristics of ITO/HBL (50 nm)/porous TiO_2 (120 nm)/F8T2^d/F8T2^s/Au with different spin-coated polymer layer thicknesses under illumination by the solar simulator (100 mW cm^{-2}, air mass 1.5).

value of about 0.8 V. The fill factor also increases from 0.38 to 0.48 with decreasing polymer thickness. The improvement of J_{SC} with decreasing polymer layer thickness is familiar from other organic photovoltaic devices.[50,51] The effect may be due to limited charge carrier mobility[52] or to optical filtering.[52] In the present case, some optical filtering is expected because the pore size, at ~10 nm, is larger than the exciton diffusion length (<5 nm). (The latter is estimated from the relative luminescence intensities of F8T2 layers on ITO and on TiO_2 substrates, using the method described in Ref. 14.) Therefore, when the pores are filled (effective polymer thickness ~60 nm) not all of the photogenerated excitons will reach the interface before recombining. Moreover, as the effective polymer thickness is increased beyond 60 nm, a layer of excess polymer is deposited on top of the porous TiO_2, which increases series resistance, thus tending to reduce J_{SC}. Increasing polymer thickness also leads to an enhanced kink effect and reduced fill factor. This is compatible with the model in Ref. 49, where it is shown that the kink feature may be enhanced by both interfacial energy mismatch and increasing transport layer thickness.

From these considerations we expect that further reducing the polymer effective thickness below 50 nm will improve photogeneration and reduce transport losses.

IV. CONCLUSIONS

We have reported on the charge separation and photovoltaic properties of TiO_2/polymer hybrid structures. Efficient photoinduced charge transfer is observed from a fluorene–thiophene copolymer, F8T2, to the TiO_2 film, while interfacial recombination is relatively slow (~100 μs). Effective penetration of the polymer into porous nanocrystalline films is achieved for films of around 100 nm thickness. In devices with the structure ITO/TiO_2/polymer/metal, significant photocurrent generation is only achieved when electrons are driven towards the ITO electrode and holes towards the metal. Therefore, it is necessary to use a high-work-function metal electrode such as Au or Pt. Inserting a thin (~100 nm) porous layer of TiO_2 into a planar TiO_2/polymer structure increases the photocurrent quantum efficiency by a factor of 5. This is attributed to the greatly increased interface area for charge separation. Device performance is improved by reducing the thickness of all layers in the system, which is explained by reduced series resistance and reduced optical filtering. The best devices have a peak external quantum efficiency of 13% and monochromatic power conversion efficiency of 1.4%. Devices with F8T2 polymer and Au contacts suffer from a poor fill factor. Comparison with other polymer-interface combinations suggests that this is due to an energy mismatch at the interface, and that contacts which allow good hole injection tend to lead to higher fill factors in this system.

ACKNOWLEDGMENTS

The authors are grateful to Mark Bernius, Mike Inbasekaran, Rob Fletcher, and Jim O'Brien of The Dow Chemical Company for providing the poly(9,9-dioctylfluorene-co-bithiophene) (F8T2) and poly(9,9-dioctylfluorene-*co*-bis-*N*,*N*′-(4-butyl phenyl)-bis-*N*,*N*′-phenyl-1,4-phenylenediamine) (PFB) samples that we have studied; to Alex Green and Emilio Palomares for the preparation of the TiO_2 paste; and to Bernard Aduda for help with SEM imaging. One of the authors (P.R.) acknowledges the Association of Commonwealth Universities for a Commonwealth Scholarship. Two of the authors (J.N. and J.R.D.) acknowledge the EPSRC for financial support.

[1] W. U. Huynh, J. J. Dittmer, and A. P. Alivisatos, Science **295**, 2425 (2002).
[2] M. Grätzel, Nature (London) **414**, 338 (2001).
[3] J.-M. Nunzi, C.R. Physique **3**, 523 (2002).
[4] J. Nelson, Mater. Today **5**, 20 (2002).
[5] C. J. Brabec, N. S. Sariciftci, and J. C. Hummelen, Adv. Funct. Mater. **11**, 15 (2001).
[6] J. J. M. Halls and R. H. Friend, in *Clean Electricity from Photovoltaics*, edited by M. D. Archer and R. D. Hill (Imperial College Press, London, 2001), p. 377.
[7] U. Bach, D. Lupo, P. Comte, J. E. Moser, F. Weissortel, J. Salbeck, H. Spreitzer, and M. Grätzel, Nature (London) **395**, 583 (1998).
[8] P. Peumans and S. R. Forrest, Appl. Phys. Lett. **79**, 126 (2001).
[9] J. Krüger, R. Plass, and M. Grätzel, Appl. Phys. Lett. **81**, 367 (2002).
[10] C. J. Brabec, S. E. Shaheen, C. Winder, N. S. Sariciftci, and P. Denk, Appl. Phys. Lett. **80**, 1288 (2002).
[11] N. C. Greenham, X. Peng, and A. P. Alivisatos, Phys. Rev. B **54**, 17628 (1996).
[12] E. Palomares, J. N. Clifford, S. A. Haque, T. Lutz, and J. R. Durrant, J. Am. Chem. Soc. **125**, 475 (2003).
[13] S. A. Haque, T. Park, A. B. Holmes, and J. R. Durrant, Chem. Phys. Chem. **4**, 89 (2003).
[14] T. J. Savenije, J. M. Warman, and A. Goossens, Chem. Phys. Lett. **287**, 148 (1998).
[15] N. A. Anderson, E. Hao, X. Ai, G. Hastings, and T. Lian, Chem. Phys. Lett. **347**, 304 (2001).
[16] A. J. Breeze, Z. Schlesinger, and S. A. Carter, Phys. Rev. B **64**, 125205 (2001).
[17] Q. Fan, B. McQuillin, D. D. C. Bradley, S. Whitelegg, and A. B. Seddon, Chem. Phys. Lett. **347**, 325 (2001).
[18] M. Y. Song, J. K. Kim, K. J. Kim, and D. Y. Kim, Synth. Met. **137**, 1387 (2003).
[19] A. C. Arango, L. R. Johnson, V. N. Bliznyuk, Z. Sclesinger, S. A. Carter, and H. H. Horhold, Adv. Mater. (Weinheim, Ger.) **12**, 1689 (2000).
[20] N. A. Anderson, E. Hao, X. Ai, G. Hastings, and T. Lian, Physica E (Amsterdam) **14**, 215 (2002).
[21] M. Kaneko, K. Takayama, S. S. Pandey, W. Takashima, T. Endo, M. Rikukawa, and K. Kaneto, Synth. Met. **121**, 1537 (2001).
[22] D. Gebeyehu, C. J. Brabec, F. Padinger, T. Fromherz, S. Spiekermann, N. Vlachopoulos, F. Kienberger, H. Schindler, and N. S. Sariciftci, Synth. Met. **121**, 1549 (2001).
[23] C. Arango, S. A. Carter, and P. J. Brock, Appl. Phys. Lett. **74**, 1698 (1999).
[24] J. S. Salafsky, Phys. Rev. B **59**, 10885 (1999).
[25] C. D. Grant, A. M. Schwartzberg, G. P. Smestad, J. Kowalik, L. M. Tolbert, and J. Z. Zhang, J. Electroanal. Chem. **522**, 40 (2002).
[26] P. A. V. Hal, M. M. Wienk, J. M. Kroon, W. J. H. V. Gennip, P. Jonkheijm, and R. A. J. Janssen, Adv. Mater. (Weinheim, Ger.) **15**, 118 (2003).
[27] P. Ravirajan, S. A. Haque, D. Poplavskyy, J. R. Durrant, D. D. C. Bradley, and J. Nelson, Thin Solid Films (in press).
[28] H. Sirringhaus, R. J. Wilson, R. H. Friend, M. Inbasekaran, W. Wu, E. P. Woo, M. Grell, and D. D. C. Bradley, Appl. Phys. Lett. **77**, 406 (2000).
[29] M. Grell, M. Redecker, K. S. Whitehead, D. D. C. Bradley, M. Inbasekaran, and E. P. Woo, Liq. Cryst. **26**, 1403 (1999).
[30] A. C. Arias, J. D. MacKenzie, R. Stevenson, J. J. M. Halls, M. Inbasekaran, E. P. Woo, D. Richards, and R. H. Friend, Macromolecules **34**, 6005 (2001).
[31] M. Redecker, M. Inbasekaran, W. W. Wu, E. P. Woo, and D. D. C. Bradley, Adv. Mater. (Weinheim, Ger.) **11**, 241 (1999).
[32] M. Inbasekaran (private communication).
[33] R. L. Willis, C. Olson, B. O'Regan, T. Lutz, J. Nelson, and J. R. Durrant, J. Phys. Chem. B **106**, 7605 (2002).
[34] L. Kavan and M. Grätzel, Electrochim. Acta **40**, 643 (1995).

[35] S. A. Haque, Y. Tachibana, D. R. Klug, and J. R. Durrant, J. Phys. Chem. B **102**, 1745 (1998).
[36] I. H. Campbell, T. W. Hagler, D. L. Smith, and J. P. Ferraris, Phys. Rev. Lett. **76**, 1900 (1995).
[37] I. Montanari, A. F. Nogueira, J. Nelson, J. R. Durrant, C. Winder, M. A. Loi, N. S. Sariciftci, and C. Brabec, Appl. Phys. Lett. **81**, 3001 (2002).
[38] S. A. Haque, Y. Tachibana, R. L. Willis, J. E. Moser, M. Grätzel, D. R. Klug, and J. R. Durrant, J. Phys. Chem. B **104**, 538 (2000).
[39] J. Krüger, R. Plass, L. Cevey, M. Piccirelli, U. Bach, and M. Grätzel, Appl. Phys. Lett. **79**, 2085 (2001).
[40] H. B. Michaelson, J. Appl. Phys. **48**, 4729 (1977).
[41] H. Ishii, K. Sugiyama, E. Ito, and K. Seki, Adv. Mater. (Weinheim, Ger.) **11**, 605 (1999).
[42] A. Ioannidis, J. S. Facci, and M. A. Abkowitz, J. Appl. Phys. **84**, 1439 (1998).
[43] D. Poplavskyy, T. Kreouzis, A. J. Campbell, J. Nelson, and D. C. C. Bradley, Mater. Res. Soc. Symp. Proc. **725**, 61 (2002).
[44] G. G. Malliaras, J. R. Salem, P. J. Brock, and C. Scott, Phys. Rev. B **58**, 13411 (1998).
[45] As measured by the Kelvin probe method; see also, T. M. Brown, J. S. Kim, R. H. Friend, F. Cacialli, R. Daik, and W. J. Feast, Appl. Phys. Lett. **75**, 1679 (1999).
[46] B. O. Aduda, P. Ravirajan, K. W. Choy, and J. Nelson, Intern. J. Photoenergy (in press).
[47] B. O. Aduda (private communication).
[48] A. Eppler (private communication).
[49] J. Nelson, J. Kirkpatrick, and P. Ravirajan, Phys. Rev. B (in press).
[50] K. Petritsch and R. H. Friend, Synth. Met. **102**, 976 (1999).
[51] C. J. Brabec, S. E. Shaheen, T. Fromherz, F. Padinger, J. C. Hummelen, A. Dhanabalan, R. A. J. Janssen, and N. S. Sariciftci, Synth. Met. **121**, 1517 (2001).
[52] M. G. Harrison, J. Grüner, and G. C. W. Spencer, Phys. Rev. B **55**, 7831 (1997).